CONF-8409103--3

SANS AND TEM STUDIES OF CARBIDE PRECIPITATION AND CREEP DAMAGE IN TYPE 304 STAINLESS STEEL*

M. H. Yoo, J. C. Ogle, J. H. Schneibel,
and R. W. Swindeman

Metals and Ceramics Division
Oak Ridge National Laboratory
Oak Ridge, Tennessee 37831

CONF-8409103--3

DE85 000933

ABSTRACT

Small-angle neutron scattering (SANS) and transmission electron microscopy (TEM) studies were performed to characterize the carbide ($M_{23}C_6$) precipitation and creep damage induced in type 304 stainless steel in the primary creep stage. The size distribution of matrix carbides evaluated from SANS analyses was consistent with TEM data, and the expected accelerated kinetics of precipitation under applied stress was confirmed. Additional SANS measurements after the postcreep solution annealing were made in order to differentiate cavities from the carbides. Potential advantages and difficulties associated with characterization of creep-induced cavitation by the SANS techniques are discussed.

1. INTRODUCTION

In contrast to pure metals and single-phase alloys, small-angle neutron scattering (SANS) intensities obtained from commercial alloys usually contain a strong scattering contribution from precipitate particles. In order to isolate the scattering intensity due to inhomogeneities induced by creep, in the case of the type 304 stainless steel, Boeuf et al. (1981) first made SANS measurements on undeformed samples aged after solution annealing treatment. The measured intensity attributable to $M_{23}C_6$ precipitates was then subtracted from the intensity measured from each crept sample (Boeuf et al., 1982). Assuming that precipitation characteristics of the carbides at a given temperature are not affected by the applied stress, Boeuf et al. (1982) attributed the net scattering intensity to creep-induced cavities.

Additional SANS measurements after postcreep solution heat treatment may provide further information to help in differentiating the carbides and cavities. This postcreep annealing method of assessing creep damage accumulated through the secondary and tertiary creep stages was discussed by Yoo et al. (1982a). The purpose of the present paper is to report on SANS measurements of creep damage accumulated in type 304 stainless steel in the primary creep stage and to discuss quantitative analyses involved in assessing creep-induced cavitation.

---

*Research sponsored by the Division of Materials Sciences, U.S. Department of Energy under contract DE-AC05-84OR21400 with the Martin Marietta Energy Systems, Inc.

2. EXPERIMENTAL PROCEDURE

2.1. Creep deformation. A reference heat of AISI type 304 stainless steel (ORNL heat 9T2796), of which creep rupture characteristics had been thoroughly investigated (Swindeman, 1979), was used for this study. Its chemical composition (wt %) is: Cr (18.6), Ni (9.7), Mn (1.22), Si (0.48), Mo (0.32), C (0.04), P (0.028), S (0.015) and Fe (balance). Creep samples were prepared from the material in the laboratory reannealed condition: 30 min at 1366 K in argon followed by a rapid cool. The resulting grain size was in the range of 80 to 120 μm. The control and crept SANS specimens were prepared from the grip and gage sections, respectively, of creep samples tested at 866 K and 138 MPa for 3450 h. These test parameters were chosen as most suitable for creep cavitation based on the analyses of creep-rupture data on this material (Swindeman, 1979).

2.2. SANS measurements. The SANS measurements were made on both the control and crept specimens, with the 30-m SANS facility at the National Center for Small-Angle Scattering Research (NCSASR). The incident neutron beam of wavelength $\lambda = 0.475$ nm was directed perpendicular to the axis of applied stress. The range of scattering vector was $\kappa = 0.032$ to $1.0\ nm^{-1}$, $\kappa = (4\pi/\lambda) \sin \theta$ where θ is the Bragg angle. Immediately after the postcreep solution heat treatment, identical to the treatment given before applying creep deformation, the annealed samples were mechanically polished using the same procedure as used for the crept specimens, and they were examined with the SANS facility under the identical operating conditions. The corrected scattered intensity from each measurement was then scaled and calibrated, according to the standard procedure at the NCSASR, to obtain the absolute coherent differential scattering cross section.

3. RESULTS AND ANALYSES

The macroscopic differential scattering cross section (heretofore simply called absolute intensity), $I \equiv d\Sigma/d\Omega$, is plotted against the magnitude of the scattering vector in Fig. 1. The sample-to-detector distances and scattering times used in the experiment are labelled in Fig. 1 for the data from gage section, both (a) as crept and (c) after anneal. Corresponding data from the control specimens are shown as (b) and (d) in Fig. 1. The straight lines with a slope of -4 in Fig. 1 indicate that in all four cases Porod's Law is well obeyed at large κ.

The product of the absolute intensity and the wave vector, $\kappa^4 I(\kappa)$, as a function of κ is a convenient basis for the analysis of size distribution of scattering centers. Such a plot is shown in Fig. 2. In each case of crept and annealed conditions, e.g. as shown in Fig. 2 for (a) and (c), the solid curve was obtained by least-square fitting of a polynominal function of eighth-order to the experimental data points. The dashed curve near the origin ($\kappa_1 < 0.032\ nm^{-1}$) shows the extrapolation based on Guinier's Law, whereas that at large diffraction vectors ($\kappa_2 \sim 0.2\ nm^{-1}$ and $\kappa_2 \sim 0.3\ nm^{-1}$, respectively, for crept and annealed cases) shows the extrapolation based on Porod's Law. Size distribution of scattering particles were then obtained by inverting the absolute intensity curves shown in Fig. 2 using the analytical method developed by Fedorova and Schmidt (1978). The same calculation procedure described by Yoo et al. (1982b) was followed here with an exception that normalization of size distribution was made with respect to the integrated intensity.

Application of an external magnetic field of 0.4 T flux density on the crept specimen did not change the absolute intensities shown in Fig. 1. Therefore,

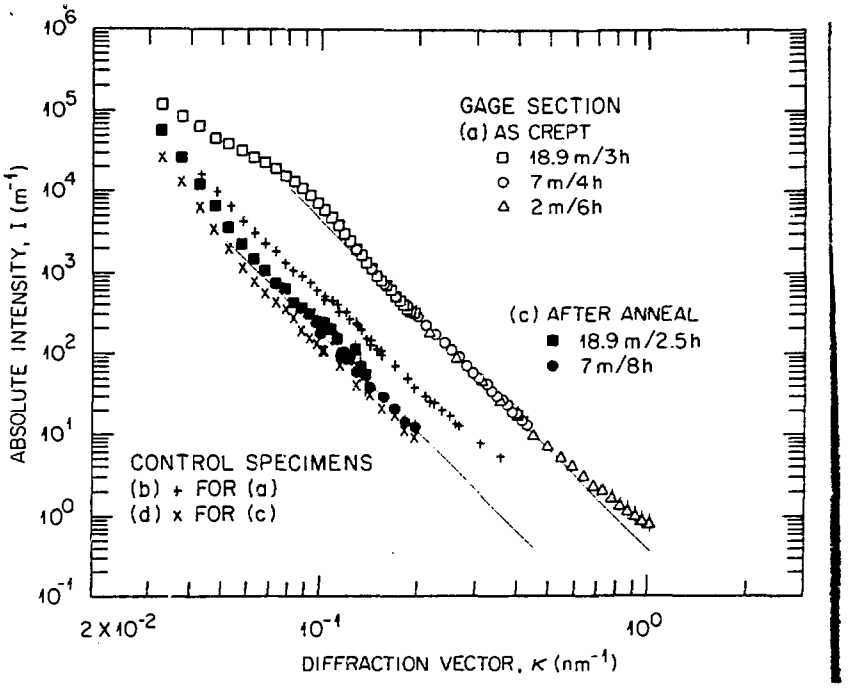

Fig. 1. The SANS absolute intensity measured in type 304 stainless steel crept at 866 K and 138 MPa for 3450 h.

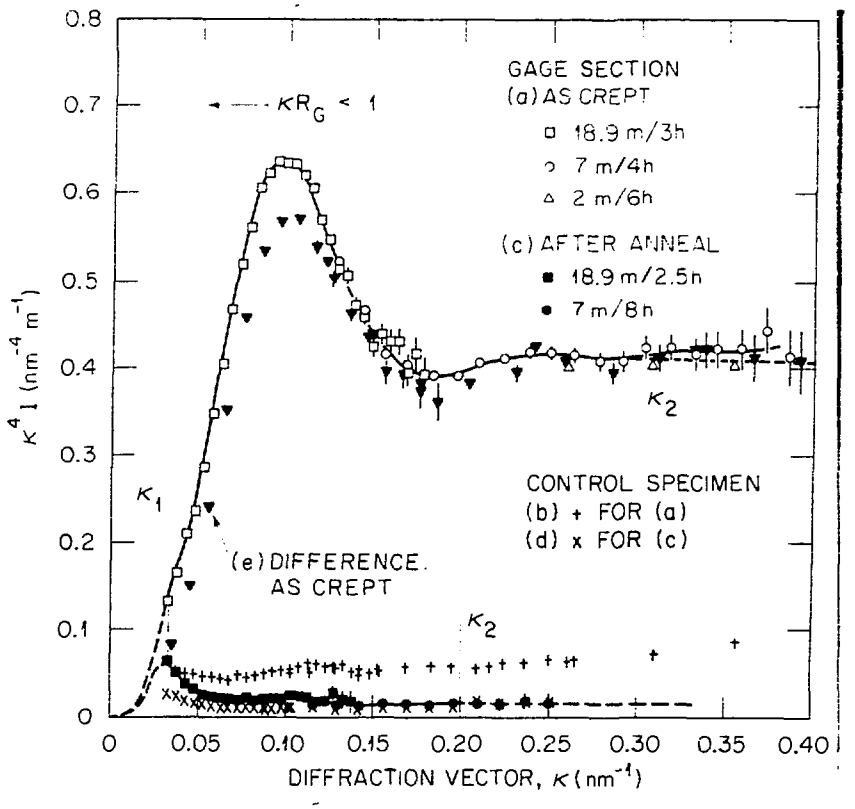

Fig. 2. Absolute intensity measured at the primary creep stage and least-square fitted polynominal curves (solid) with the Guinier and Porod extrapolations (dashed).

nuclear scattering cross section which is proportional to the differential homogeneous scattering length density, $(\Delta\rho)^2$, is assumed to be the physical source of scattering. The magnitudes of $\Delta\rho$ used for the present two-phase analysis are 3.4×10^{14} m^{-2} and 7.4×10^{14} m^{-2} for $M_{23}C_6$ carbides and cavities, respectively. Either the precipitates or cavities were assumed to be randomly distributed and of spherical shape with sharp interface. The size distribution of the carbides obtained from the curves (a), (b), and (c) are shown by the solid curves in Fig. 3. The dashed curves (e) and (f) were obtained based on the differences in scattering intensities, as recorded on the position sensitive detector, between the crept and control specimens.

In general, the shape of a size distribution at the small size range depends very sensitively on the choice of κ_2, where the Porod extrapolation is taken (Fig. 2). For the cases of (a), (b), and (e) $\kappa_2 = 0.2$ nm^{-1} was used, whereas $\kappa_2 = 0.14$ nm^{-1} was used for (c) and (f). The normalization constant was obtained in reference to the integrated intensity. Therefore, the ordinate scale of Fig. 3, the magnitude of number density, depends on the basic strength of neutron scattering, i.e. $\Delta\rho$, assumed in the two-phase model. The mean diameter, $\bar{D}$, the total number density, N, and the volume fraction, $\Delta V/V$ are tabulated in the insert of Fig. 3 for the cases of the control (b), as crept (a), and postanneal specimens (f) when scatterers are assumed as $M_{23}C_6$ carbides.

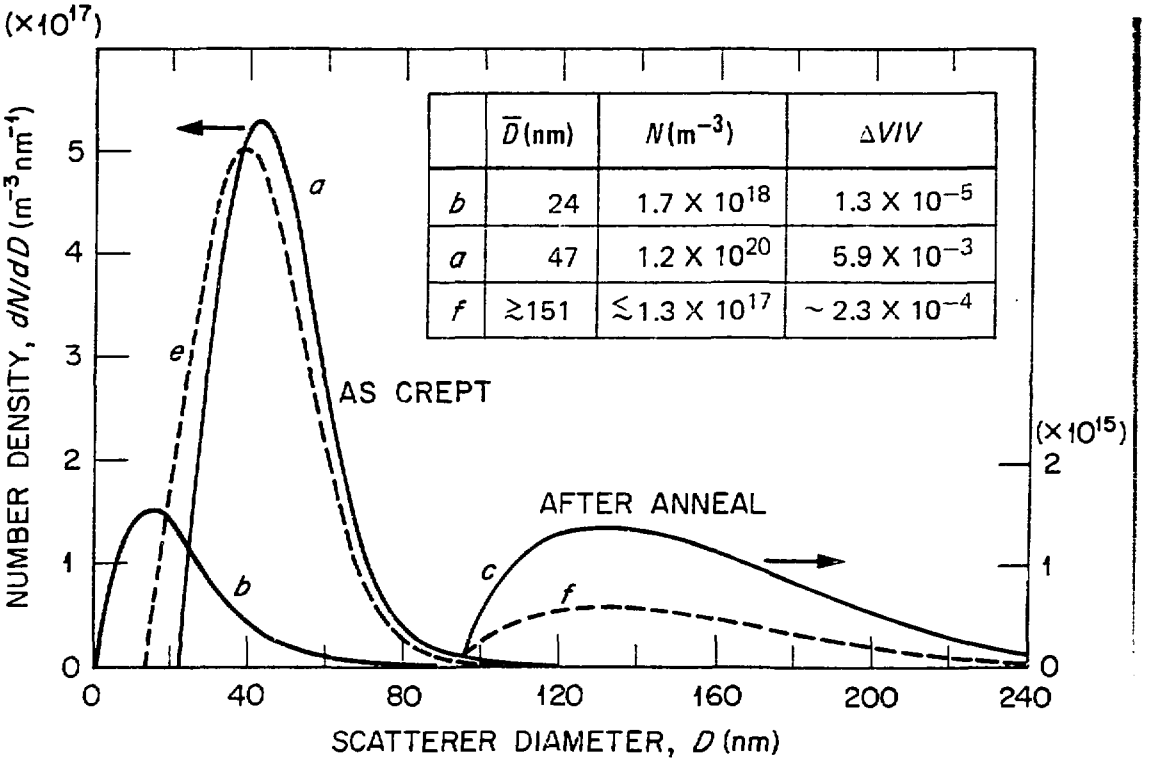

	$\bar{D}$(nm)	$N(m^{-3})$	$\Delta V/V$
b	24	1.7×10^{18}	1.3×10^{-5}
a	47	1.2×10^{20}	5.9×10^{-3}
f	≳151	≲1.3×10^{17}	~2.3×10^{-4}

Fig. 3. Size distributions of $M_{23}C_6$ carbides in (b) the control, (a) as crept, and (c) after anneal specimens. The dashed curves (e) and (f) represent the net stress-induced damage.

4. DISCUSSION

Three most important prerequisites for a fully quantitative interpretation of SANS data are: (i) a sufficient strength of scattering intensity, (ii) a wide range of κ to cover the Guinier and Porod regions, and (iii) direct evidence of the nature of scattering centers. In the case of (a), gage section as crept, all three conditions were fully satisfied. The carbide size distribution with $\bar{D}$ = 47 nm shown by (a) in Fig. 3 is consistent with the size range of matrix carbides, 20 to 80 nm, estimated by TEM investigation. The matrix carbides appear cuboidal, and they were distributed quite randomly throughout the matrix. In contrast, grain-boundary carbides were found to be more irregular in shape and larger in size, about 200 to 600 nm. However, these large grain-boundary carbides were mostly outside the maximum size limit detectable by the 30-m SANS facility, viz. $D_{max} \simeq 200$ nm. Within the size resolution limit of SANS technique and the sampling limit of TEM observation, both the mean diameter and number density of matrix carbides estimated by the two techniques are consistent throughout the primary, secondary, and tertiary creep stages.

It is known that growth kinetics of matrix precipitates is generally enhanced by deformation at elevated temperatures (Ilschner, 1973). In the case of matrix carbides ($M_{23}C_6$) in type 304 stainless steel, it has been established by Etienne et al. (1975) and Swindeman et al. (1977) that dislocation substructure developed during creep offers more heterogeneous sites for nucleation and hence accelerates both the nucleation and growth of carbides. According to the modified kinetics of carbide precipitation shown in Fig. 43 by Swindeman et al. (1977), this creep-enhanced carbide formation is expected to be very pronounced at 866 K beyond about 10^3 h. This is evidenced by a comparison of the curves (a) and (b) in Fig. 1 or 2. The difference in test temperature, 866 K, from the center of gage section to the grip section, from which the control specimen was prepared, was monitored to be only about —1%. Our TEM analysis of the control specimen confirms heterogeneous distribution of matrix carbides in the size range consistent with $\bar{D}$ = 24 nm shown by (b) of Fig. 3. The net difference in scattering intensity as shown by (e) of Fig. 2 indicates that the scattering contribution from carbides in the crept specimens comes primarily from the creep-induced matrix carbides. Therefore, the superposition method proposed by Boeuf et al. (1982) cannot be applied to separate the scattering contribution from creep cavities and that from creep-induced precipitates.

As for the net scattering after the solution heat treatment (30 min at 1366 K), only qualitative interpretation is possible because of difficulties in meeting the three prerequisites. A number of possible sources may be responsible for the curve (f) of Fig. 3. First, the residual grain-boundary carbides surviving the heat treatment may be the source. Second, the residual precipitates could be an intermetallic second phase such as σ-phase. Third, cavities may be the scatterers. There are three possible ways in which some creep cavities could remain after the annealing: (i) large cavities shrink to the detectable size range, (ii) grain boundaries migrate away, and intergranular cavities are left behind in the matrix; or (iii) cavitation process becomes irreversible and sintering does not occur due to solute segregation to cavity surfaces. The table in Fig. 3 shows the number density and the volume fraction of $M_{23}C_6$ carbides. If cavities contribute to the curve (f), then N is less than 2.7×10^{16} m^{-3} and $\Delta V/V \simeq 4.8 \times 10^{-5}$.

The solution heat treatment eliminated essentially all the creep-induced matrix carbides, as evidenced by TEM observations. In some isolated cases,

precipitate particles and cavity like contrast of about 100 nm in diameter or larger were observed using a 1 MeV high voltage electron microscope (HVEM). In all cases, however, these appear as holes intersecting the foil surfaces. They could have been enlarged from either smaller cavities or precipitates because of the etching effect of foil preparation. In any case, the number density of holes or precipitates observed using TEM is consistent with the SANS data.

Both the difficulty in applying the superposition method (Boeuf et al., 1982) and the ambiguity in interpretation of the postcreep annealing results can be partially eliminated by lowering the carbon content of the material. A SANS study of creep cavitation in a model ternary alloy with a lower carbon content (<40 ppm C) is underway, and the results will be reported elsewhere.

ACKNOWLEDGMENTS

We are deeply indebted to S. Spooner and other staff members of the National Center for Small-Angle Scattering Research for allowing extra beam time with the 30-m SANS facility in order that our specimens could be annealed and measured under the same conditions and settings of the facility. The NCSASR is sponsored by the National Science Foundation through an interagency agreement with the Department of Energy. We are also indebted to H. Trinkaus and C. T. Liu for helpful discussion on the manuscript, W. H. Farmer for his skillful performance in specimen preparation to meet our experimental schedule, and to C. L. Dowker for preparing the manuscript.

REFERENCES

Boeuf, A., Coppola, R., Rustichelli, F., Zambonardi, F., Melone, S., Maggi, S., and Puliti, P. (1981). Small-angle neutron scattering investigation of $M_{23}C_6$ precipitation in AISI type 304 stainless steel. J. Appl. Cryst. 14, 337–344.

Boeuf, A., Coppola, R., Rustichelli, F., Zambonardi, F., Melone, S., and Puliti, P. (1982). Small-angle neutron scattering investigation of creep damage in AISI type 304 stainless steel. In: Mechanical behavior and nuclear applications of stainless steel at elevated temperatures. Edited by D. J. Hatfull (The Metals Society, London) 94–98.

Etienne, C.F., Dortland, W., and Zeedijk, H.B. (1975). On the capability of austenitic stainless steel to withstand cyclic deformation during service at elevated temperature. In: Creep and fatigue in elevated temperature applications (Institute of Mechanical Engineers, London) 225.1–.9.

Ilschner, B. (1973). Hochtemperatur-Plastizität. (Springer-Verlag, Berlin) 164–169.

Swindeman, R.W. (1979). Analysis of creep-rupture data for reference heat of type 304 stainless steel (Heat 9T2796). ORNL-5565, 59pp.

Swindeman, R.W., Bhargava, R.K., Sikka, V.K., and Moteff, J. (1977). Substructures developed during creep and cyclic tests of type 304 stainless steel (Heat 9T2796). ORNL-5293, 30pp.

Yoo, M.H., Ogle, J.C., Schneibel, J.H., and Swindeman, R.W. (1982a). Small-angle neutron scattering study of creep deformation and fracture of type 304 stainless steel. In: The strength of metals and alloys — 6th. Edited by G. F. Gifkins (Pergamon Press, Melbourne) 677–682.

Yoo, M.H., Ogle, J.C., Borie, B.S., Lee, E.H., and Hendricks, R.W. (1982b). Small-angle neutron scattering study of fatigue induced cavities in nickel. Acta Metall. 30, 1733–1742.